Pressure Dependence of the Contact Angle

ARTICLE *in* THE JOURNAL OF PHYSICAL CHEMISTRY B · JULY 2007

Impact Factor: 3.3 · DOI: 10.1021/jp071372y · Source: PubMed

3 AUTHORS, INCLUDING:

Tanvir I. Farouk
University of South Carolina
34 PUBLICATIONS **409** CITATIONS

SEE PROFILE

Charles Albert Ward
University of Toronto
141 PUBLICATIONS **2,594** CITATIONS

SEE PROFILE

Pressure Dependence of the Contact Angle

Jiyu Wu, T. Farouk, and C. A. Ward*

Thermodynamics and Kinetics Laboratory, Department of Mechanical and Industrial Engineering, University of Toronto, Toronto, Canada M5S 3G8

Received: February 17, 2007; In Final Form: March 26, 2007

When a liquid and its vapor contact a smooth, homogeneous surface, Gibbsian thermodynamics indicates that the contact angle depends on the pressure at the three-phase line of an isothermal system. When a recently proposed adsorption isotherm for a solid−vapor interface is combined with the equilibrium conditions and the system is assumed to be in a cylinder where the liquid−vapor interface can be approximated as spherical, the contact-angle−pressure relation can be made explicit. It indicates that a range of contact angles can be observed on a smooth homogeneous surface by changing the pressure at the three-phase line, but it also indicates that the adsorption at the solid−liquid interface is negative, and leads to the prediction that the contact angle increases with pressure. The predicted dependence of the contact angle on pressure is investigated experimentally in a system that has an independent mechanism for determining when thermodynamic equilibrium is reached. The predictions are in agreement with the measurements. The results provide a possible explanation for contact angle hysteresis.

1. Introduction

Recently, a method was proposed for determining the surface tensions of solid−liquid and solid−vapor interfaces.[1] The method is based on an equilibrium adsorption isotherm for the solid−vapor interface and Gibbsian thermodynamics.[2] The isotherm expression was obtained by approximating the adsorbate as molecular clusters with a maximum of one cluster adsorbed at an adsorption site. The expression obtained had the essential characteristic of predicting a finite amount adsorbed at the saturation-vapor pressure. The isotherm was examined using data from the literature for five vapor−solid systems[3−8] and was found to give an accurate description of the amount adsorbed for each.[1] Gibbsian thermodynamics was applied by taking a particular definition of the position of the solid−liquid and solid−vapor interfaces. In each case, it was assumed the position was such that the excess number of moles of the solid component vanished. When the isotherm relation was combined with the necessary conditions for equilibrium, it was found that in an isothermal, solid−fluid system, the pressure, in either fluid phase, could be treated as the independent thermodynamic variable of the contact angle, θ, and of the surface tensions at the solid−vapor and solid−liquid interfaces, $\gamma_{[1]}^{SV}$, $\gamma_{[1]}^{SL}$ respectively, where the bracketed subscript indicates the chosen interface position. This conclusion is contrary to the idea that the contact angle is a material property of a solid−fluid system, and means one can observe a range of equilibrium contact angles on a smooth, homogeneous surface by simply changing the pressure at the three-phase line (see below).

The approach was examined by determining the surface tension of the basal plane of carbon in the absence of adsorption, $\gamma_{[1]}^{S0}$ from adsorption measurements made with either benzene or *n*-hexane adsorbing.[3−6] The expression for $\gamma_{[1]}^{SV}$ was determined first, and then the limit was taken in which the vapor-phase pressure went to zero. The value of $\gamma_{[1]}^{S0}$ determined from these independent adsorption measurements was found to be the same, which it should be since $\gamma_{[1]}^{S0}$ is a material property of the solid.[1]

However, when this approach is applied for a liquid partially filling a cylinder that has a radius small enough so the liquid−vapor interface can be approximated as spherical, the adsorption is predicted to be negative at the solid−liquid interface and is predicted to be positive at the solid−vapor interface. Although it is easy to understand how the Gibbs definition of the interface position can lead to negative values of the adsorption,[9,10] a negative adsorption means the effect of adsorption is predicted to increase $\gamma_{[1]}^{SL}$ as the pressure at the three-phase line is increased. As a result, the value of θ is also predicted to increase with increasing pressure. We examine these conclusions in a series of experiments with H_2O contacting (Pyrex 7740 borosilicate) glass. It is observed that θ increases with pressure and that the change in pressure required to change the contact angle a given amount can be predicted. As discussed below, the fact that θ is predicted and observed to increase with pressure due to negative adsorption at the solid−liquid interface provides a possible explanation for contact angle hysteresis.

2. The Independent Variable of the Contact Angle

Suppose a single component liquid and its vapor are in contact with a smooth, homogeneous, rigid, and nondissolving solid, and they are exposed to a gravitational field and maintained isothermal. At the three-phase line, we suppose a contact angle is formed and equilibrium exists in the system. This requires the chemical potentials of the molecules in phase j at height z in the field, $\mu^j(z)$ to satisfy[2,11]

$$\mu^j[T, x^j(z)] + Wgz = \lambda \tag{1}$$

where j is L, V, LV, SV, or SL indicating the liquid, vapor, liquid−vapor, solid−vapor, or solid−liquid interface; x^j is the ratio of the pressure in phase j to the saturation vapor pressure,

* Corresponding author phone: 416-978-4807; fax: 416-978-7322; e-mail: ward@mie.utoronto.ca.

10.1021/jp071372y CCC: $37.00
Published on Web 05/12/2007

P_s; T is the temperature of the equilibrium system; W is the molecular weight of the fluid, g is the gravitational intensity; and λ is a constant.

At the liquid−vapor interface, following Gibbs, we use the surface-of-tension approximation. Then, if the position of the three-phase line is denoted as z_3, and the principal curvatures of the liquid−vapor interface at the three-phase line as $C_1(z_3)$ and $C_2(z_3)$, the Laplace equation applied at the three-phase line may be written as follows:[2,11]

$$x^{V}(z_3) - x^{L}(z_3) = \frac{\gamma^{LV}}{P_s}[C_1(z_3) + C_2(z_3)] \tag{2}$$

where a curvature is taken as positive if the vapor is inside the interface.

Equilibrium at the three-phase line requires the Young equation to be satisfied. For the position of the dividing surface that we have adopted, the Young equation may then be written as shown:

$$\gamma^{SV}_{[1]} - \gamma^{SL}_{[1]} = \gamma^{LV}\cos\theta \tag{3}$$

If the molar specific volume of the liquid at saturation is denoted as v_f, and the liquid phase has an isothermal compressibility of κ_T, then provided $|\kappa_T P_s[x^L(z_3) - 1]| \ll 1$, the chemical potential in the liquid may be expressed

$$\mu^{L}[T, x^{L}(z_3)] = \mu(T, P_s) + v_f P_s[x^{L}(z_3) - 1] \tag{4}$$

If the vapor phase is approximated as an ideal gas, then

$$\mu^{V}[T, x^{V}(z_3)] = \mu(T, P_s) + k_b T \ln[x^{V}(z_3)] \tag{5}$$

where k_b is the Boltzmann constant.

For the isothermal system we consider, the Gibbs adsorption equation at the solid−liquid interface may be written as

$$d\gamma^{SL}_{[1]} = -n^{SL}_{[1]} d\mu^{SL} \tag{6}$$

and at the solid−vapor interface

$$d\gamma^{SV}_{[1]} = -n^{SV}_{[1]} d\mu^{SV} \tag{7}$$

When eq 1 is applied at the three-phase line in the liquid, at the solid−vapor interface, at the solid−liquid interface, and in the vapor phase at the three-phase line, one finds

$$\mu^{L}[P^{L}(z_3)] = \mu^{SV}(z_3) \tag{8}$$

$$\mu^{L}[P^{L}(z_3)] = \mu^{SL}(z_3) \tag{9}$$

$$\mu^{L}[P^{L}(z_3)] = \mu^{V}[P^{V}(z_3)] \tag{10}$$

From eqs 4, 6, and 9:

$$d\gamma^{SL}_{[1]} = -n^{SL}_{[1]} v_f P_s dx^{L}(z_3) \tag{11}$$

and similarly, from eqs 4, 7 and 8:

$$d\gamma^{SV}_{[1]} = -n^{SV}_{[1]} v_f P_s dx^{L}(z_3) \tag{12}$$

Equations 11 and 12 indicate that $\gamma^{SV}_{[1]}$ and $\gamma^{SL}_{[1]}$ may each be viewed as having $x^L(z_3)$ as its independent, thermodynamic variable. After taking the total differential of eq 3, assuming γ^{LV} is only a function of temperature, and using eqs 11 and 12, one finds

$$d\cos\theta[x^{L}(z_3)] = \left(\frac{v_f P_s}{\gamma^{LV}}\right)(n^{SL}_{[1]} - n^{SV}_{[1]})dx^{L}(z_3) \tag{13}$$

Therefore, there is a functional relation between θ and $x^L(z_3)$:

$$\theta = \theta[x^{L}(z_3)] \tag{14}$$

Equation 13 indicates the net adsorption $(n^{SL}_{[1]} - n^{SV}_{[1]})$ is the mechanism that relates θ with $x^L(z_3)$.

Since the vapor has been approximated as an ideal gas, one finds from eqs 4, 5, and 10

$$x^{V}(z_3) = \exp\left[\frac{v_f}{v_g}[x^{L}(z_3) - 1]\right] \tag{15}$$

where the v_g is molar specific volume of the vapor at saturation. Thus, only one of the bulk-phase pressures at the three-phase line may be treated as independent.

2.1. Adsorption Isotherm at the Solid−Vapor Interface. In reference 1, an expression for $n^{SV}_{[1]}$ was obtainined by supposing the adsorbate could be approximated as molecular clusters, that a maximum of one cluster could adsorb per site, and that a maximum of ζ molecules could be in any one cluster. Clusters with different numbers of molecules were viewed as different species, and the canonical ensemble was employed to determine the expression for the isotherm. In addition to ζ, the isotherm expression contains three parameters: the number of adsorption sites per unit area, M; and the temperature-dependent parameters, α and c.

$$n^{SV}_{[1]} = \frac{Mc\alpha x^{V}[1 - (1 + \zeta)(\alpha x^{V})^{\zeta} + \zeta(\alpha x^{V})^{1+\zeta}]}{(1 - \alpha x^{V})[1 + (c - 1)\alpha x^{V} - c(\alpha x^{V})^{1+\zeta}]} \tag{16}$$

The isotherm expression was examined by determining if the values of the parameters could be selected so the calculated amount adsorbed was in agreement with that measured. The systems examined included benzene and n-hexane adsorbing on (primarily) the basal plane of carbon;[3-6] water vapor adsorbing on silica (TK 800) and on alumina (Baikowski CR 1);[7] and benzene adsorbing on "pulverized" quartz.[8]

A study of the role played by the maximum number of molecules in a cluster, ζ, indicated that the agreement between the measurements and the calculations remained unchanging (provided it was above a threshold value), even if ζ was allowed to approach infinity.[1] This allows the ζ-isotherm to be simplified without reducing the accuracy of the calculations. When ζ is allowed to approach infinity, eq 16 reduces to

$$n^{SV}_{[1]}[x^{V}(z_3)] = \frac{Mc\alpha x^{V}(z_3)}{[1 - \alpha x^{V}(z_3)][1 + (c - 1)\alpha x^{V}(z_3)]} \tag{17}$$

The comparison between the measured amount adsorbed and that calculated from eq 17 indicated the isotherm gave an accurate description of the amount adsorbed for each of the systems listed in Table 1. The error between the calculated and measured values for each of these systems was less than 1.1%.

The adsorption at the solid−liquid interface may be expressed in terms of $n^{SV}_{[1]}[x^V(z_3)]$ and the function $\cos\theta[x^L(z_3)]$; after

rearranging eq 13, one finds

$$n_{[1]}^{SL}[x^V(z_3)] = n_{[1]}^{SV}[x^V(z_3)] + \frac{\gamma^{LV}}{v_f P_s}\frac{d\cos\theta[x^L(z_3)]}{dx^L(z_3)} \quad (18)$$

Conceptually, the description of the interfacial properties is now complete. All four interfacial thermodynamic properties, θ, $x^V(z_3)$, $n_{[1]}^{SV}[x^V(z_3)]$, and $n_{[1]}^{SL}[x^L(z_3)]$ may be viewed as having $x^L(z_3)$ as their independent thermodynamic variable. However, the explicit form of the expression indicated in eq 14 cannot be determined until the experimental circumstance is fully defined.

2.2. Negative Adsorption at the Solid−Liquid Interface When the Liquid−Vapor Interface is Spherical. Now we consider the circumstance that will be examined experimentally. Suppose the fluid is held in a right-circular cylinder and that the cylinder radius, r_{cy}, is sufficiently small so the Bond number ($\equiv Wgr_{cy}^2/v_f\gamma^{LV}$) is small compared to unity (see Figure 1). The liquid−vapor interface can then be approximated as spherical,[12] and the two curvatures of the liquid−vapor interface become equal and are denoted $C(z_3)$. This information is sufficient to determine explicitly the relation indicated in eq 14.

From geometry, one finds

$$\cos\theta[x^L(z_3)] = r_{cy}C(z_3) \quad (19)$$

and

$$\cos\theta = \frac{2r_{cy}z_m}{z_m^2 + r_{cy}^2} \quad (20)$$

where z_m is the meniscus height. An expression for $\cos\theta[x^L(z_3)]$ may be obtained by combining eqs 2, 15, and 19:

$$\cos\theta[x^L(z_3)] = \left(\frac{P_s r_{cy}}{2\gamma^{LV}}\right)\left[\exp\left(\frac{v_f}{v_g}[x^L(z_3) - 1]\right) - x^L(z_3)\right] \quad (21)$$

Equation 21 is the explicit form of eq 14: provided r_{cy} and the fluid properties are known at T, eq 21 indicates $x^L(z_3)$ may be viewed as the independent variable and θ predicted as a function of $x^L(z_3)$.

The value of θ can range from zero to π. The values of $x^L(z_3)$ corresponding to each of these angles are referred to as x_w^L and x_π^L respectively. For a particular fluid and cylinder size, their values may be determined from eq 21. For the temperatures we consider, $v_f/v_g \ll 1$, the exponential in eq 21 can be expanded, and the expressions for x_w^L and x_π^L determined:

$$1 - \frac{2\gamma^{LV}}{P_s r_{cy}} \le x^L(z_3) \le 1 + \frac{2\gamma^{LV}}{P_s r_{cy}} \quad (22)$$

Equation 22 defines the range of $x^L(z_3)$ for which the contact angle of a particular fluid can exist in a certain sized cylinder. If $x^L(z_3)$ is less than x_w^L the liquid evaporates, and if $x^L(z_3)$ is greater than x_π^L, the vapor condenses.[1]

The expression for $n_{[1]}^{SL}[x^V(z_3)]$, in terms of $x^L(z_3)$, may be obtained by combining eqs 15, 18, and eq 21:

$$n_{[1]}^{SL}[x^L(z_3)] = n_{[1]}^{SV}[x^L(z_3)] + \frac{r_{cy}}{2v_f}\left[\frac{v_f}{v_g}\exp\left(\frac{v_f}{v_g}[x^L(z_3) - 1]\right) - 1\right] \quad (23)$$

If the material of the cylinder is specified, and its adsorption properties are known (i.e., the values of M, c, and α), then eqs 15, 17, and 23 can be used to calculate the adsorption at the solid−vapor and solid−liquid interfaces as a function of $x^L(z_3)$. The type of results obtained for $n_{[1]}^{SV}(x_3^L)$ is illustrated for water adsorbing on silica in Figure 2A. The values of $x^L(z_3)$ considered are those in the range indicated in eq 22. These values of $n_{[1]}^{SV}[x^L(z_3)]$ can then be used in eq 23 and the values of $n_{[1]}^{SL}[x^L(z_3)]$ calculated, see Figure 2B. Note $n_{[1]}^{SL}[x^L(z_3)]$ is

TABLE 1: Parameters of the Isotherm Given in Eq 17 for Benzene and *n*-Hexane Adsorbing on Graphitized Carbon[a] and Water Vapor Adsorbing on Silica (TK800), and on Alumina (Baikowski CR1)[b]

system	t(°C)	M (kmol/m^2)	c	α	$\gamma_{[1]}^{s0}$ (kg/s^2)
benzene on basal plane of C	20	3.96×10^{-9}	115.97	0.8473	0.091
		$\pm 8.5 \times 10^{-11}$	±15.04	±0.007	±0.003
n-hexane on basal plane of C	20	3.43×10^{-9}	875.46	0.8211	0.088
		$\pm 3.9 \times 10^{-11}$	±60.02	±0.005	±0.001
water on SiO_2	30	5.25×10^{-9}	15.54	0.9447	0.145
		$\pm 7.2 \times 10^{-11}$	±1.79	±0.0019	±0.003
water on Al_2O_3	20	1.03×10^{-8}	43.28	0.8399	0.209
		$\pm 3.2 \times 10^{-10}$	±12.18	±0.0090	+0.012/ −0.014

[a] Obtained from the data of Isirikyan and Kiselev.[3] [b] Obtained from the data reported by Naono and Hakuman.[7,1]

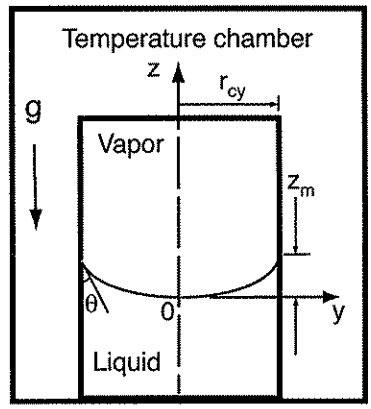

Figure 1. Definition of the parameters describing a fluid partially filling a right, circular cylinder.

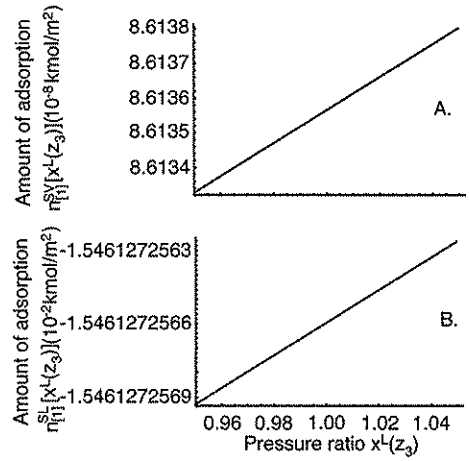

Figure 2. Amount predicted to be adsorbed at the solid−vapor and solid−liquid interfaces when water is held in a silica(TK 800) cylinder of 0.56 mm radius, maintained at 30 °C, and $x^L(z_3)$ is in the range where the contact angle can exist.

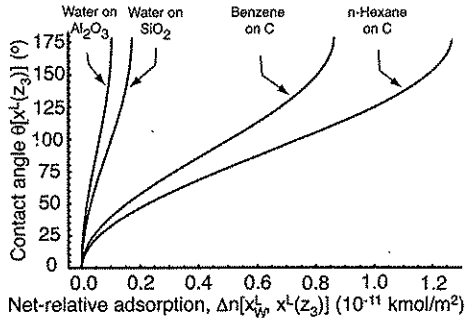

Figure 3. Contact angle as a function of the adsorption relative to that at wetting for different fluids in cylinders constructed of different materials, but each cylinder having a radius of 0.56 mm. The fluid–material combinations are water in an alumina cylinder, maintained at 20 °C; water in a silica cylinder, maintained at 30 °C; benzene in a carbon tube with the basal plane of carbon exposed to the benzene and maintained at 20 °C; and *n*-hexane in a carbon tube with the basal plane of carbon exposed to the *n*-hexane and maintained at 20 °C.

predicted to be negative in sign and 5 orders of magnitude larger in absolute value than $n_{[1]}^{SV}[x^V(z_3)]$; also, that as $x^L(z_3)$ is increased $n_{[1]}^{SL}[x^L(z_3)]$ becomes less negative, but for the range of possible $x^L(z_3)$ values, $n_{[1]}^{SL}[x^L(z_3)]$ remains negative. Since $n_{[1]}^{SL}[x^L(z_3)]$ is negative, eq 11 indicates $\gamma_{[1]}^{SL}[x^L(z_3)]$ increases with $x^L(z_3)$. This is in contrast to the predicted effect of adsorption at the solid–vapor interface. Since $n_{[1]}^{SV}[x^L(z_3)]$ is positive, $\gamma_{[1]}^{SV}[x^L(z_3)]$ is predicted to decrease with an increase in $x^L(z_3)$. These predictions may be viewed as a direct consequence of the position chosen for the dividing surfaces, and will be explored experimentally.

For a spherical liquid–vapor interface, these results may be used to determine the predicted effect of pressure on θ. As indicated in Figure 2, the net adsorption $(n_{[1]}^{SL}[x^L(z_3)] - n_{[1]}^{SV}[x^V(z_3)])$ is negative, and from Figure 2, it is negative for all values of $x^L(z_3)$ for which the contact angle can exist (see eq 22). Then, from eq 18

$$\frac{d\cos\theta[x^L(z_3)]}{dx^L(z_3)} < 0 \tag{24}$$

Thus, the prediction is that θ increases with $x^L(z_3)$.

The amount by which θ increases with a change in $x^L(z_3)$ depends on the substrate material. The net adsorption relative to that at wetting, $\Delta n[x_W^L, x^L(z_3)]$ is defined as

$$\Delta n[x_W^L, x^L(z_3)] \equiv (n_{[1]}^{SL}[x^L(z_3)] - n_{[1]}^{SV}[x^L(z_3)]) - [n_{[1]}^{SL}(x_w^L) - n_{[1]}^{SV}(x_w^L)] \tag{25}$$

As $x^L(z_3)$ changes from x_w^L to x_π^L, $\Delta n[x_w^L, x^L(z_3)]$ changes from zero to $\Delta n[x_w^L, x_\pi^L]$. This changes θ from zero to π. Although physically it is the net-relative adsorption that gives rise to a particular value of θ, the calculations are performed in the inverse order. For a given value of θ, the value of $\Delta n[x_w^L, x^L(z_3)]$ is calculated in a series of steps: first, the value of x_w^L is calculated from eq 21 by setting $\theta[x^L(z_3)]$ equal to zero and replacing $x^L(z_3)$ with x_w^L; second, the value of x_w^V is obtained from eq 15; third, $n_{[1]}^{SV}(x_w^V)$ is determined from eq 17 using the values of M, c, and α tabulated in Table 1; fourth, the value of $n_{[1]}^{SL}(x_w^L)$ is obtained from eq 23; this allows $(n_{[1]}^{SL}[x_w^L(z_3)] - n_{[1]}^{SV}[x_w^L(z_3)])$ to be calculated corresponding to a given value of θ.

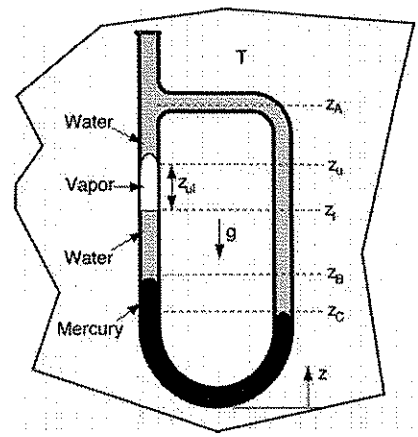

Figure 4. Capillary tube formed into a "b"-shape; containing Hg and, except for the water–vapor phase in the left branch, is otherwise filled with water. The b-tube was closed at the top by a valve (not shown), and surrounded by a temperature reservoir. The system is shown in a nonequilibrium configuration.

By choosing another value of $\theta[x^L(z_3)]$, and following a similar procedure, the value of $\Delta n[x_w^L, x^L(z_3)]$ may be obtained. As illustrated in Figure 3 for four different fluids in cylinders constructed of different materials and each cylinder having a radius of 0.56 mm, as the net-relative adsorption increases, the contact angle is predicted to also increase in each case. The net-relative adsorption required to produce a given value of θ differs greatly between fluid-substrate combinations. For example, the value of the net-relative adsorption required to produce a contact angle of $\pi/2$ when *n*-hexane is in contact with the basal plane of carbon is greater by more than an order of magnitude than the value required to produce the same angle when water is in an alumina cylinder.

Provided $x^L(z_3)$ is in the range defined by eq 22, Ward and Wu[1] found $\gamma_{[1]}^{SV}[x^L(z_3)]$ is essentially constant and has a value very near that of γ^{LV}

$$\gamma_{[1]}^{SV}[x^L(z_3)] = \gamma^{LV} \tag{26}$$

and at the solid–liquid interface

$$\gamma_{[1]}^{SL}[x^L(z_3)] = \gamma^{LV}(1 - \cos\theta[x^L(z_3)]) \tag{27}$$

Since θ is predicted to increase with $\Delta n[x_w^L, x^L(z_3)]$, eq 27 indicates $\gamma_{[1]}^{SL}$ also *increases* with the net-relative adsorption.

3. Experimental Investigation of a Water-Glass System

A capillary tube that has been formed into the b-shape (see Figure 4) has been used to examine the predicted relation of θ to $x^L(z_3)$ (see eq 21). As will be seen, because of the gravitational field, the liquid-phase pressure at the lower three-phase line, z_l, is greater than that at the upper three-phase line, z_u, and the value of θ at each of these positions can be directly measured by measuring the meniscus height (see eq 20). Further, by increasing the length of the vapor phase, the pressure at the lower three-phase line can be increased relative to that at the upper three-phase line. Thus, the difference in θ between the upper and lower three-phase lines is predicted to increase as the length of the vapor phase is increased.

3.1. Criterion for Thermodynamic Equilibrium. As indicated in Figure 4, Hg was placed at the bottom of a "b"-shaped capillary tube, and produced Hg columns on each side of the capillary. These Hg columns provide a measurement of the relative pressure at the bottom of each water column, and they

can provide a criterion for equilibrium of the system. We apply the necessary conditions for equilibrium to show that when the system has reached equilibrium, the height of the Hg columns will be the same, independently of the presence of the vapor phase on one side of the b-tube.

We neglect any dissolution of the Hg into the water and adsorption of the Hg onto the glass. Thus, for the Hg phase, as a body, to be unmoving, the force on the Hg—pressure on the water side of the interface times the projected interface area of the Hg-water interface, πr_{cy}^2—at z_C and at z_B, must have the same value (see Figure 4). Under equilibrium conditions, the temperature is uniform in a system subjected to a gravitational field.[2,11] Therefore, P_s is uniform in the b-tube, and since the pressures at z_C and at z_B are the same (for the Hg phase to be unmoving), $x^L(z_C)$ and $x^L(z_B)$ must have the same value at these positions. Thus, one of the necessary conditions for equilibrium of the Hg is

$$x^L(z_C) = x^L(z_B) \tag{28}$$

We show this means the heights of the Hg columns, z_C and z_B must be the same, independently of the presence of the vapor phase on one side of the b-tube.

From eqs 1 and 4 at z_B in the left branch of the b-tube, one finds

$$\mu(T, P_s) + v_f P_s(x^L(z_B) - 1) + Wgz_B = \lambda \tag{29}$$

and at z_C in the right branch

$$\mu(T, P_s) + v_f P_s(x^L(z_C) - 1) + Wgz_C = \lambda \tag{30}$$

After subtracting eq 30 from eq 29:

$$x^L(z_B) - x^L(z_C) = \frac{Wg}{v_f P_s}(z_C - z_B) \tag{31}$$

and taking advantage eq 28, one finds from eq 31

$$z_B = z_C \tag{32}$$

Thus the prediction is that when the system comes to equilibrium, the Hg-column heights on the two sides of the b-tube will be the same. This conclusion is investigated experimentally below.

3.2. Contact Angle as a Function of Height in the Capillary. If eqs 1 and 4 are combined and applied at a reference height z_r and at an arbitrary height z, one finds

$$\mu(T, P_s) + v_f P_s[x^L(z_r) - 1] + Wgz_r = \lambda \tag{33}$$

and

$$\mu(T, P_s) + v_f P_s[x^L(z) - 1] + Wgz = \lambda \tag{34}$$

After subtracting eq 33 from eq 34, the expression for the pressure ratio as a function of z and z_r is obtained

$$x^L(z) = x^L(z_r) + \frac{Wg}{v_f P_s}(z_r - z) \tag{35}$$

An examination of eq 35 indicates that the difference in pressure between z_r and z is predicted to be the same as it would have been had the vapor phase been replaced by liquid (see below).[11,13]

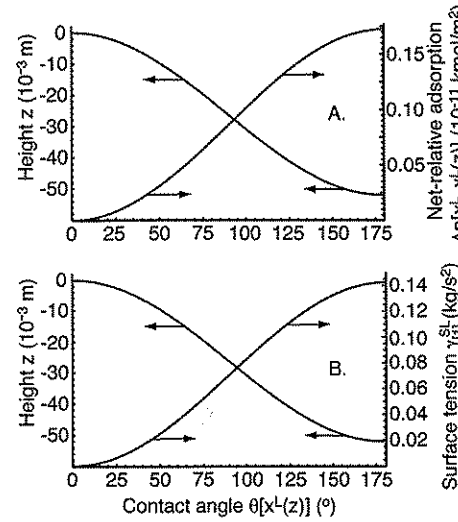

Figure 5. Independent variable x^L acts as a parametric variable and is used to calculate properties that would exist if a three-phase line were placed at height z in a 0.56 mm-radius silica capillary that was filled with water and maintained at 30 °C. (A) One curve indicates the predicted dependence of θ on height. The other curve indicates the adsorption relative to that at wetting ($\Delta n(x_w^L, x^L(z))$, eq 25) that would give rise to $\theta(z)$. Height is measured from the height at wetting. (B) The value of $\gamma_{[1]}^{SL}$ as a function of θ and as a function of height for the same capillary as in A.

Since $x^L(z)$ is independent of the presence of the vapor phase, the contact angle that would exist if there were a vapor phase present, and its three-phase line at height z can be obtained. We take the origin of the height measurement to be the position where the wetting condition is reached. The value of $x^L(0)$ may be determined from eq 21:

$$1 = \left(\frac{P_s r_{cy}}{2\gamma^{LV}}\right)\left[\exp\left(\frac{v_f}{v_g}[x^L(0) - 1]\right) - x^L(0)\right] \tag{36}$$

Its value may be determined numerically, and substituted into eq 35:

$$x^L(z) = x^L(0) - \frac{Wgz}{v_f P_s} \tag{37}$$

The expression for $\theta(z)$ may then be obtained by substituting eq 37 into eq 21:

$$\cos\theta[x^L(z)] = \frac{P_s r_{cy}}{2\gamma^{LV}}\left[\exp\left(\frac{v_f}{v_g}\left[x^L(0) - 1 - \frac{Wgz}{v_f P_s}\right]\right) - x^L(0) + \frac{Wgz}{v_f P_s}\right] \tag{38}$$

The type of results obtained from eq 38 is illustrated in Figure 5A. The observed contact angle is predicted to increase with depth in the capillary. The net-relative adsorption that gives rise to this dependence is indicated by the other curve in this figure. It is calculated from eq 25 for water in a 0.56 mm radius silica capillary for each value of θ indicated in Figure 5A, following the procedure outlined above. This curve depends on the substrate material (see Figure 3). In Figure 5B, the calculated value of $\gamma_{[1]}^{SL}$ obtained from eq 27 is shown. Note the close correlation between $\gamma_{[1]}^{SL}$ and the net-relative adsorption shown in Figure 5A.

3.3. Observed Equilibrium Configurations of H_2O in the b-Tube. In preparation for an experiment with the b-tube (0.56 mm-radius, Pyrex 7740 borosilicate glass), water was deionized

TABLE 2: Summary of Experimental Observations When the System Was in Equilibrium

measured separation distance of three-phase lines (±0.01 mm)	measured upper meniscus height (±0.01 mm)	measured lower meniscus height (±0.01 mm)	measured upper contact angle (°)	measured lower contact angle (°)	predicted separation distance of three-phase lines (mm)
7.35	0.436	0.21	14.2 ± 2.3	48.9 ± 2.5	8.08 ± 1.11
14.45	0.482	0.128	8.6 ± 2.2	64.2 ± 2.4	14.33 ± 1.13
23.86	0.486	0.012	8.1 ± 2.2	87.5 ± 2.1	24.49 ± 1.11

(Corning LD-2a filter), distilled (Corning AG-3ADA), and nanofiltered until its resistivity reached 18 M Ω-cm (Branstead Nanopure Bioresearch). After these operations, the surface tension of the purified water was 0.0712 ± 0.0008 kg/s^2 at 25 °C. Water prepared in this fashion was used for rinsing. After this preparation, the water to be used as the experimental fluid was transferred to a degassing flask where it was exposed to a vacuum overnight while being stirred.

The b-tube was cleaned using a three-stage procedure before each experiment. In each stage it was filled with a solvent and held for 24 h. The solvents were acetone (Aldrich HPLC grade), an aqueous detergent (Alconox biodegradable) solution, and chromic and sulfuric acid (Fisher Chromerge). After each stage, the b-tube was thoroughly rinsed with the prepared water.

The cleaned b-tube was put in a special vacuum filling apparatus that allowed it to be vacuumed for a period of 24 h, and, without exposure to air, to be partially filled with Hg using a small plastic tube that could go inside the b-tube. It was further filled with degassed water, and finally, a volume of water vapor was formed in the b-tube, as indicated in Figure 4. Once a vapor phase of the desired length had been formed, a ball valve at the top of the b-tube (not shown) was closed without forming another vapor phase. Thus, when the filling procedure had been completed, the configuration was similar to that shown in Figure 4, but we emphasize that the configuration shown is a non-equilibrium one. Afterward, the filled b-tube was enclosed in a clear plastic container and maintained at 33 ± 1.5 °C as it evolved toward equilibrium. The b-tube could be viewed from outside the container with a cathetometer, and the meniscus heights of both the water−vapor and the mercury−water interfaces could be measured to an accuracy of ± 10 μm using a cathetometer.

A series of three experiments was conducted with the vapor-phase having different lengths (see Table 2). The heights of the Hg columns on each side of the b-tube were monitored during each experiment to determine when a system had reached equilibrium. The type of results observed are shown in Figure 6 for the experiment in which the vapor-phase was ~15 mm in length. Note that, initially, there was a clear difference in the Hg-column heights, but the system slowly evolved until there was no longer any measurable difference between their heights, and it remained there once the system had reached this configuration. In each experiment, the system was observed to evolve to a configuration in which the Hg columns had the same heights.

That the system was in equilibrium when the Hg columns had the same height was confirmed by the observed values of the dynamic contact angles that were measured as a function of time. Each day, the meniscus heights at the upper and lower three-phase lines were measured, and the contact angles were calculated using eq 20. The results of the experiment when the vapor-phase had a length of ~15 mm are summarized in Figure 7. As seen in Figure 7, there was no longer any measurable change in the contact angles after 17 days. This corresponds to the time required for the system to reach a configuration in which the Hg columns had the same height (see Figure 6). In Figure 8, a photograph of the equilibrium system containing a vapor phase ~15 mm in length is shown. The Hg columns may be seen to be of the same height, and θ_l is seen to be greater than θ_u.

In Table 2, the equilibrium contact angles at the three-phase lines of each experiment are recorded. In each case, θ_l was greater than θ_u, and the difference in these equilibrium contact angles increased as the vapor-phase length was increased. The position in the capillary, relative to the wetting position, at which a particular value of θ is predicted to be observed may be calculated by substituting the observed values of θ into eq 38 to obtain z_u and z_l. Then the predicted heights may be subtracted to obtain the predicted difference in height of the three-phase lines, z_{ul}^P. A measurement of the equilibrium separation distance between the two three-phase lines of a vapor phase, z_{ul}^M was made with the cathetometer in each experiment. In Figure 9, the predicted and measured values of the separation distance are compared. Note there was no measurable difference between that predicted, z_{ul}^P, and that measured, z_{ul}^M.

For each experiment, the value of the contact angle at the lower three-phase line may be predicted from the measurement of the meniscus height at the upper three-phase line and the separation distance between these positions. For the temperatures considered, $v_f/v_g \ll 1$. This allows the exponential in eq 21 to be expanded. After keeping only the first two terms of the

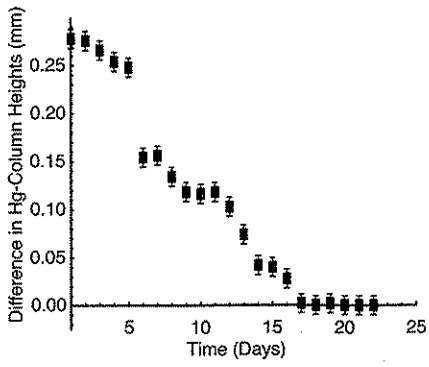

Figure 6. Measured difference in the height of the mercury columns for the experiment in which the vapor phase was ~15 mm in length.

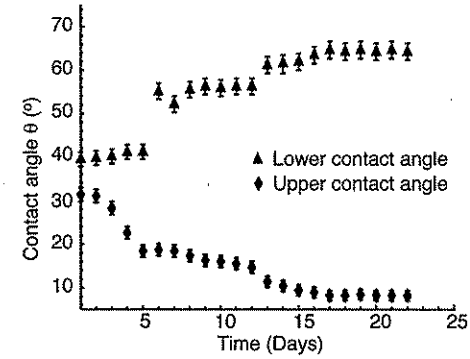

Figure 7. Measured dynamic contact angles as a function of time for the experiment in which the vapor-phase had a length of ~15 mm (see Table 2) are shown.

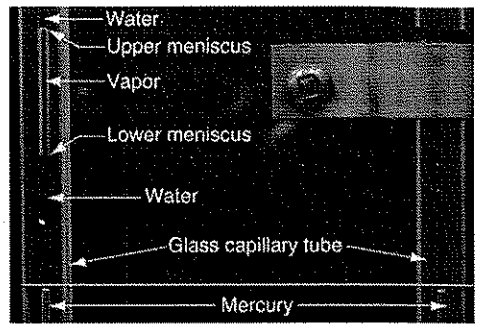

Figure 8. Photograph of the system when a vapor-phase that was ~15 mm in length was present in the left branch of the b-tube (see Figure 4) and the system had reached equilibrium. Note the heights of the Hg-water interfaces on both sides of the b-tube have the same value, and the contact angle at the lower water–vapor interface is larger than that at the upper water–vapor interface (see Table 2).

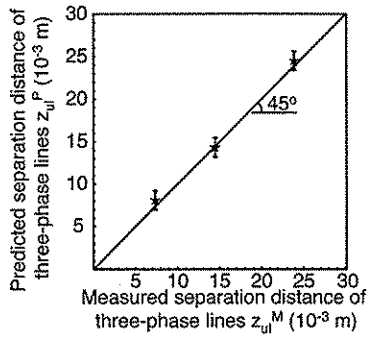

Figure 9. Comparison of the measured and predicted separation distances of the three-phase lines of each vapor phase in the experiments. The contact angles at the upper and lower three-phase lines are listed in Table 2.

expansion and simplifying the result by neglecting v_f/v_g compared to unity, one finds

$$\cos\theta[x^{L}(z_3)] = \left(\frac{P_s r_{cy}}{2\gamma^{LV}}\right)[1 - x^{L}(z_3)] \tag{39}$$

When eq 39 is applied at the upper and lower three-phase lines of the b-tube, and the two equations subtracted, the result may be written

$$\cos\theta[x^{L}(z_l)] = \cos\theta[x^{L}(z_u)] + \left(\frac{P_s r_{cy}}{2\gamma^{LV}}\right)[x^{L}(z_u) - x^{L}(z_l)] \tag{40}$$

After applying eq 37 at the upper and at the lower three-phase lines of the b-tube, and subtracting the two equations, one finds

$$x^{L}(z_u) - x^{L}(z_l) = -\frac{Wgz_{ul}}{v_f P_s} \tag{41}$$

Equation 41 may be substituted into eq 40 to obtain

$$\cos\theta[x^{L}(z_l)] = \cos\theta[x^{L}(z_u)] - \left(\frac{Wgr_{cy}z_{ul}}{2v_f\gamma^{LV}}\right) \tag{42}$$

As seen in eq 40, $\cos\theta[x^{L}(z_l)] - \cos\theta[x^{L}(z_u)]$ is predicted to be proportional to the difference in pressure, $x^{L}(z_u) - x^{L}(z_l)$. This difference in pressure is proportional to the separation distance, z_{ul}, between the upper and lower three-phase lines (eq 41). Therefore, $(\cos\theta[x^{L}(z_l)] - \cos\theta[x^{L}(z_u)])$ is predicted to be proportional to the separation distance, z_{ul}.

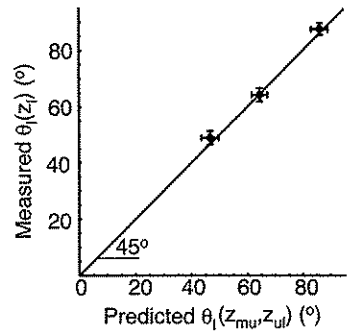

Figure 10. Comparison of the measured and predicted contact angle at the lower three-phase line.

By measuring the meniscus height at the upper three-phase line, z_{mu}, the value of $\theta[x^{L}(z_u)]$ can be determined using eq 20. The separation distance between the three-phase lines, z_{ul}, was measured in each experiment (see Table 2). When $\theta[x^{L}(z_u)]$ and z_{ul} are inserted in eq 42, the value of $\theta[x^{L}(z_l)]$ at the lower three-phase can be predicted. The result of this procedure is shown in Figure 10 along with measured values of the lower contact angle in each of the three experiments. Note there was no measurable disagreement between the predictions and the measurements.

4. Discussion and Conclusion

When a liquid and its vapor contact a solid surface under isothermal conditions, and the Gibbs dividing surfaces[2] are placed so there is no adsorption of the solid component at either the solid–liquid or the solid–vapor interface, the equilibrium conditions at the three-phase line indicate a relation exists between θ and $x^{L}(z_3)$ (see eq 14). This relation can be made explicit if the liquid and its vapor partially fill a right circular cylinder of sufficiently small radius so the liquid–vapor interface may be approximated as spherical (see eq 21). If an adsorption isotherm at the solid–vapor interface is incorporated in the analysis, the equilibrium adsorption at the solid–liquid interface can be predicted (see eqs 16 and 23).

The ζ-isotherm has been recently proposed,[1] and it has significant experimental support when applied at a solid–vapor interface. If it is used with the equilibrium conditions to calculate the amount adsorbed at the solid–liquid interface, the adsorption there is found to be negative (see Figure 2). It is understood that this results from the position chosen for the Gibbs dividing surface, and that another position could be chosen so the adsorption would be positive;[9] however, the question would remain of whether the dividing-surface approach could be used reliably to predict observable quantities.

One prediction of this approach is that since $n_{[1]}^{SL}$ is negative, $\gamma_{[1]}^{SL}$ *increases* with an increase in $x^{L}(z_3)$ (see eq 11). This is in contrast with the effect of adsorption at the solid–vapor interface where adsorption tends to lower $\gamma_{[1]}^{SV}$. However, when $x^{L}(z_3)$ is in the range where θ can exist (see eq 22), $\gamma_{[1]}^{SV}$ is essentially constant.[1] From both of these statements and the Young equation (eq 3), one concludes that θ increases with $x^{L}(z_3)$, but the amount by which θ increases for a given change in $x^{L}(z_3)$ depends on the M, c, and α (the adsorption isotherm parameters) for the substrate (see Figure 3).

The effect of solid–liquid adsorption on $\gamma_{[1]}^{SL}$ and on θ was examined in the experiments. The expression for $x^{L}(z)$ in the *liquid* phase of the b-tube, shown schematically in Figure 4, indicates that $x^{L}(z)$ is the same as it would have been had the vapor phase in the left-branch been replaced by liquid (see eq 35). In other words, the value of $x^{L}(z)$ in the liquid phase is

independent of the presence of the vapor phase, and increases with depth at the same rate as that in the right-branch of the b-tube (see eq 37). This predicted pressure profile in the liquid phase is surprising, and when it was first introduced,[11] an objection was raised that claimed the pressure profile was "clearly nonphysical since the pressure at the base of the capillary filled with liquid differs significantly when part of the liquid above is replaced by vapor".[14] Since the Hg is present at the bottom of the b-tube, this contention can be tested. The two branches of the b-tube are connected; thus, both branches of the b-tube have the same pressure at one height (z_A in Figure 4). If the contention were valid, the Hg column in the left-branch would have been greater in height than in the one in the right-branch of the b-tube, but such a configuration was never observed under equilibrium conditions. The observed equilibrium configuration was always one in which the Hg columns had the same height, as predicted (see Figure 8). This gives experimental support to the expression for $x^L(z)$ given in eq 35, and it was used in further analysis.

One of the important properties of the $x^L(z)$ expression is its independence from the presence of the vapor phase. This allows the value of x^L that would exist at height z in the left branch of the b-tube (see Figure 4) to be predicted. From this value of x^L, three interface characteristics at z can be predicted: the value of θ that would exist there if a vapor phase were present and its associated three-phase line were at z, the value of $\gamma^{SL}_{[1]}$, and—provided the adsorption properties (M, c, and α) of the solid were known—the net adsorption relative to that at wetting, $\Delta n[x^L_w, x^L(z)]$ (see eq 25). The predicted results for a silica capillary are shown in Figure 5A and B. Note that θ, $\gamma^{SL}_{[1]}$, and $\Delta n[x^L_w, x^L(z)]$ increased with depth because $x^L(z)$ increased with depth.

Experiments were conducted to examine these calculations by introducing vapor phases of different lengths into the b-tube and waiting for the system to come to equilibrium in each case. The Hg-column heights provided a criterion for equilibrium. Once equilibrium had been reached, the meniscus height at the upper and lower three-phase lines were measured, and eq 20 applied to determine the values of θ at each of these positions. These values of θ were used in eq 38 to calculate the height of each three-phase line, and these values were subtracted to determine the separation distance between the three-phase lines. This distance is independent of the coordinate-system origin, and could be directly compared with the measured separation distance between the three-phase lines. The comparison is shown in Figure 9. Note there was no measurable difference between the predicted and measured values of these separation distances.

The data was examined in a second way. The difference in the values of $\cos\theta[x^L(z_3)]$ between the upper and lower three-phase lines is predicted to be proportional to the pressure difference between these positions (see eq 40), and this pressure difference can be calculated from the measured separation distance and the predicted pressure profile (see eq 41). Further, $\theta[x^L(z_u)]$ can be determined by measuring the upper meniscus height. Thus, the contact angle at the lower three-phase line can be predicted from measurements of the upper-meniscus height and the separation distance between the three-phase lines. These predictions are shown in Figure 10, and as seen there, close agreement was found between the predictions and the measurements.

The analysis of the experimental results suggests that although the adsorption at the solid−liquid interface is predicted to be negative, the Gibbs dividing-surface approach leads to valid predictions of the pressure dependence of the contact angle.

We note that in order for the vapor phase to defy gravity and come to equilibrium at some intermediate position, rather than at the top of the capillary, all of the conditions for equilibrium must be satisfied. This is an important consideration for $n^{SL}_{[1]}$ because its value was calculated from the equilibrium conditions. No independent isotherm relation is available for the solid−liquid interface. The adsorption there, $n^{SL}_{[1]}$, was calculated from the ζ-isotherm and the conditions for equilibrium. This means the calculations give the value $n^{SL}_{[1]}$ must have if the system is to come to equilibrium. If the adsorption at the solid−liquid interface does not reach this value, then no equilibrium state would be observed. When water was replaced by ethanol and the experiments repeated, our observations were that an equilibrium state could not be achieved, although the same rigorous cleaning procedure had been followed. The vapor phase of ethanol slowly rose to the top of the capillary.

One of the clear implications of these results is related to contact angle hysteresis. A common observation is that a droplet on an inclined surface in a gravitational field exhibits a difference in the value of the contact angle at the advancing and receding edges of the droplet. The usual assumption is that this results from substrate roughness and, or heterogeneity.[15] However, this explanation implicitly assumes that under equilibrium conditions, there is only one contact angle for a liquid−substrate system. Johnson and Dettre stated this view strongly: contact angle "hysteresis is not a feature of [the] Gibbs theory which predicts" on a smooth, homogeneous surface "one and only one stable angle for a given system".[16]

As indicated above, Gibbsian thermodynamics would predict one and only one contact angle, only if x^L were uniform around the droplet periphery. Clearly, for a droplet on an inclined plane in a gravitational field, x^L would be larger at the advancing edge of the droplet than at the receding edge. We have shown experimentally that a contact angle difference of 79° exists for the water−(borosilicate) glass surface when the pressure difference between the two three-phase lines is 2.386 cm H_2O (or 235 Pa), also that with the assumption of the glass surface being smooth and homogeneous, Gibbsian thermodynamics can be used to predict the observed hysteresis (see Figures 9 and 10). This suggests that contact angle hysteresis on a smooth, homogeneous surface results from a difference in pressure between the leading and receding edges of the droplet. And on a heterogeneous and/or rough surface, the pressure dependence of the contact angle would make some contribution to contact angle hysteresis.

Acknowledgment. We gratefully acknowledge the support of this work by the Natural Sciences and Engineering Research Council of Canada.

References and Notes

(1) Ward, C. A.; Wu, Jiyu. *J. Phys. Chem. B* **2007**, *111*, 3685.

(2) Gibbs, J. W. *Trans. Conn. Acad. Arts Sci.* **1876**, *3*, 108; republished as *The Scientific Papers of J. Willard Gibbs*; Bumstead, H. A.; Van Name, R. G. Eds.; Dover: NY, 1961; Vol. 1, pp 219.

(3) Isirikyan, A. A.; Kiselev, A. V. *J. Phys. Chem.* **1961**, *65*, 601.

(4) Polley, M. H.; Schaeffer, W. D.; Smith, W. R. *J. Phys. Chem.* **1953**, *57*, 469.

(5) Avgul, N. N.; Kiselev, A. V. In *Chemistry and Physics of Carbon*; Walker, P. L., Jr. Ed.; Marcel Dekker Inc.: NY, 1970; Vol. 6, pp 1.

(6) Spencer, W. B.; Amberg, C. H.; Beebe, R. A. *J. Phys. Chem.* **1958**, *62*, 719.

(7) Naono, H.; Hakuman, M. *J. Colloid Interface Sci.* **1991**, *145*, 405.

(8) Naono, H.; Hakuman, M.; Nakai, K. *J. Colloid Interface Sci.* **1994**, *165*, 532.

(9) Defay, R.; Prigogine, I.; Bellemans, A.; Everett, D. H. *Surface Tension and Adsorption*; Longmans, Green and Co.: London, 1966; pp 24.
(10) Rowlinson, J. S.; Widon, B. *Molecular Theory of Capillarity*; Clarendon Press: Oxford, 1982; pp. 31.
(11) Ward, C. A.; Sasges, M. R. *J. Chem. Phys.* **1998**, *109*, 3651.
(12) Sasges, M. R.; Ward, C. A.; Azuma, H.; Yoshihara, S. *J. Appl. Phys.* **1996**, *79*, 8770.
(13) Sasges, M. R.; Ward, C. A. *J. Chem. Phys.* **1998**, *109*, 3661.
(14) Blokius, E. M. *J. Chem. Phys.* **2000**, *112*, 5511.
(15) Hiemenz, P. C. *Principles of Colloid and Surface Chemistry*; Marcel Dekker Inc.: New York, 1977; pp 228.
(16) Johnson, R. E.; Dettre, R. H. In *Surface and Interface Science*; Matijevic, E. Ed.; J. Wiley and Sons: 1969; Vol. 2, pp 86.